Supplemental Material for "Cavity QED based on strongly localized modes: exponentially enhancing single-atom cooperativity"

Qian Bin,[1,2] Ying Wu,[2] Jin-Hua Gao,[2] Aixi Chen,[3] Franco Nori,[4,5,6] and Xin-You Lü[2,*]

[1]*College of Physics, Sichuan University, Chengdu 610065, China*
[2]*School of Physics and Institute for Quantum Science and Engineering, Huazhong University of Science and Technology, and Wuhan Institute of Quantum Technology, Wuhan 430074, China*
[3]*Key Laboratory of Optical Field Manipulation of Zhejiang Province, Department of Physics, Zhejiang Sci-Tech University, Hangzhou 310018, China*
[4]*Theoretical Quantum Physics Laboratory, Cluster for Pioneering Research, RIKEN, Wako-shi, Saitama 351-0198, Japan*
[5]*Quantum Information Physics Theory Research Team, Quantum Computing Center, RIKEN, Wakoshi, Saitama, 351-0198, Japan*
[6]*Physics Department, The University of Michigan, Ann Arbor, Michigan 48109-1040, USA*

(Dated: August 15, 2025)

Overview of the Supplemental Material

In this Supplemental Material, we present the electric field intensity distributions of the resonant modes with different transverse and longitudinal mode orders for different types of Fabry–Pérot cavities. We studied the effects of the geometric structure of these cavities on the resonant frequencies, quality factor, and effective mode volume, by performing finite-element simulations. These simulations are carried out under the condition of perfect electrical conductor and utilize a 2D axisymmetric formulation. This supplemental material contains four parts: I. A discussion on the properties of the plane-plane Fabry–Pérot cavity. II. Discussion on the properties of winged symmetric confocal Fabry–Pérot cavities with two different sizes; III. A discussion on the properties of the winged microdome Fabry–Pérot cavities; IV. Discussions of local coupling strength and Purcell enhancement analyzed via the simplified single high-Q mode approximation and the Green's dyadic approach.

I. PLANE-PLANE FABRY–PÉROT CAVITY

In Fig. S1, we present the properties of the plane-plane Fabry–Pérot cavity. Figures S1(a) and S1(b) display the electric field intensity distributions for modes with small longitudinal mode orders k, where the transverse mode orders are $m = 0$ and $m = 1$, respectively. The corresponding resonant frequencies are approximatively $\omega_a^{(k)}/2\pi = ck/(2\eta L)$, as indicated in Figs. S1(c) and S1(f). Here, the longitudinal mode order k is an integer that determines the number of half-wavelengths along the cavity's axis, c is the speed of light in a vacuum, η is the vacuum refractive index, and L is the distance between the two cavity mirrors. There are some deviations between the simulation results and those derived from the resonant frequency formula, likely because the mesh is not sufficiently refined, particularly around the cavity and boundary regions, which might not capture the electromagnetic field variations accurately, affecting the accuracy of the simulation results. Increasing the radius of the cavity mirrors r does not significantly alter the eigenvalues of the resonant modes, as evidenced by the eigenfrequency spectra in Figs. S1(c) and S1(f). However, both the quality factor Q and effective mode volume V are significantly affected by the wing width d. Figures S1(d,e) and S1(g,h) show the effects of r/L on the quality factor Q and mode volume V for different values of m and k. Here for large Q, the mode volume can be approximately reduced to $V = \int_{\mathcal{V}} \epsilon(\mathbf{r})|\mathbf{E}(\mathbf{r})|^2/\max[\epsilon(\mathbf{r})|\mathbf{E}(\mathbf{r})|^2]d^3\mathbf{r}$ [1, 2], where $\mathbf{E}(\mathbf{r})$ represents the electric field, and $\mathcal{V}$ is the quantization volume of the electromagnetic field. Both the Q and V increase with increasing the mirror radius r for all longitudinal mode orders k, indicating that improving the Q-factor is accompanied by an increase in V. Obviously, as the mirror radius of the plane-plane cavity increases, the distribution range of the electric field intensity of the modes becomes larger because the increase in mirror radius does not correspondingly localize the electric field distribution.

*Electronic address: xinyoulu@hust.edu.cn

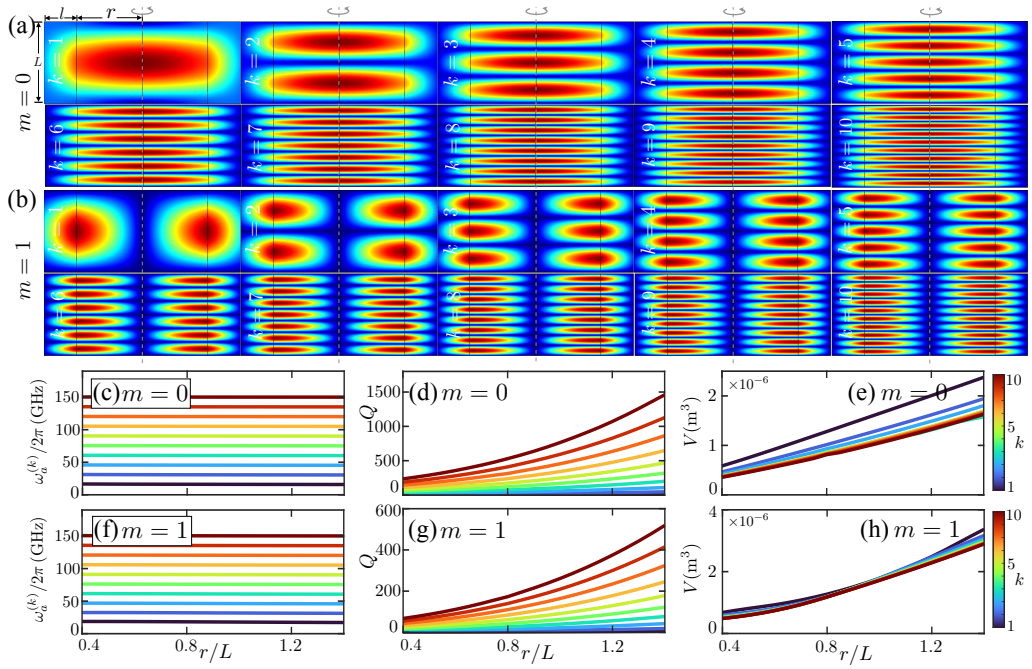

FIG. S1: (a-b) Electric field intensity distributions of the resonant modes with different transverse mode orders m and longitudinal mode orders k of the plane-plane Fabry–Pérot cavity when the radius $r = 0.8L$. Here, r is the radius of the cavity mirrors and l is the width of perfectly matched layers. (c-h) Resonant frequencies $\omega_a^{(k)}/2\pi$, quality factor Q, and mode volume V of the plane-plane Fabry–Pérot cavity versus r/L for different m and k. The geometric parameters of the cavity used here are: $L = 1\,\mathrm{cm}$ and $l = 0.4L$.

II. WINGED SYMMETRIC CONFOCAL FABRY–PÉROT CAVITY

In Fig. S2, we present the properties of a specially designed Fabry–Pérot cavity with special geometric structures. This Fabry–Pérot cavity consists of two mirrors with additional wings, where the maximum and minimum distances between the mirrors are L and h, respectively, with d representing the width of the wings. When the wing width $d = 0$, the cavity reduces to a standard symmetric confocal cavity, where both mirrors are curved with equal radii of curvature, and the cavity length L equals the radius of curvature of the mirrors, i.e., $R_1 = R_2 = L$. The resonant frequencies of a standard symmetric confocal Fabry–Pérot cavity are given by $\omega_a^{(k)}/2\pi = c[k + (m + 1)/2]/(2\eta L)$, where m represents the number of pitch lines in the direction of the argument. The additional $+1$ arises from the Guoy phase shift, a specific phase change associated with the focus of Gaussian beams in the cavity. The resonant frequencies depend not only on the longitudinal mode order k but also significantly on the geometry of the cavity through L, as well as the mode shapes described by the transverse mode order m. However, the resonant frequencies $\omega_a^{(k)}$ are almost unaffected by the change of the wing width d, as shown in Figs. S2(c) and S2(f).

Figures S2(a) and S2(b) show the electric field intensity distributions of the resonant modes of the cavity for different longitudinal mode orders k and transverse mode orders m. These electric field intensity distributions are primarily confined to the central region of the cavity, rather than the wings. Additionally, we also present the effects of the wing width d/L on the quality factor Q and the mode volume V. The mode volume V remains unchanged with increasing d, as shown in Figs. S2(e) and S2(h). This is because the special geometry of the winged cavity enhances the electric field intensities but hardly modifies the electric field distributions, as demonstrated by the similar electric field intensities in Figs. S2(a) and S2(b), even with changes in d. The quality factor Q, however, varies with increasing d for most modes, as shown in Figs. S2(d) and S2(g). For modes with the longitudinal mode orders $k = 1$ when $m = 0$ and $k = 1, 2$ when $m = 1$ (corresponding to the subwavelength light modes), the Q-factor improves almost exponentially with increasing d, as indicated by the asterisks in Figs. S2(d) and S2(g). From Figs. S2(d,e) and S2(g,h), it is evident that the typical trade-off between Q and V, which exists in the plane-plane Fabry–Pérot cavity, is overcome in this specially designed cavity. As a result, the Q/V ratio and single-atom cooperativity parameter C can also improve almost exponentially with increasing d in this cavity QED system, as discussed in the main text.

In the main text and the preceding discussions, we mainly focused on centimeter-scale cavities. Here, we extend our study to explore the properties of micrometer-scale winged symmetric confocal Fabry–Pérot cavities. Figure S3 shows

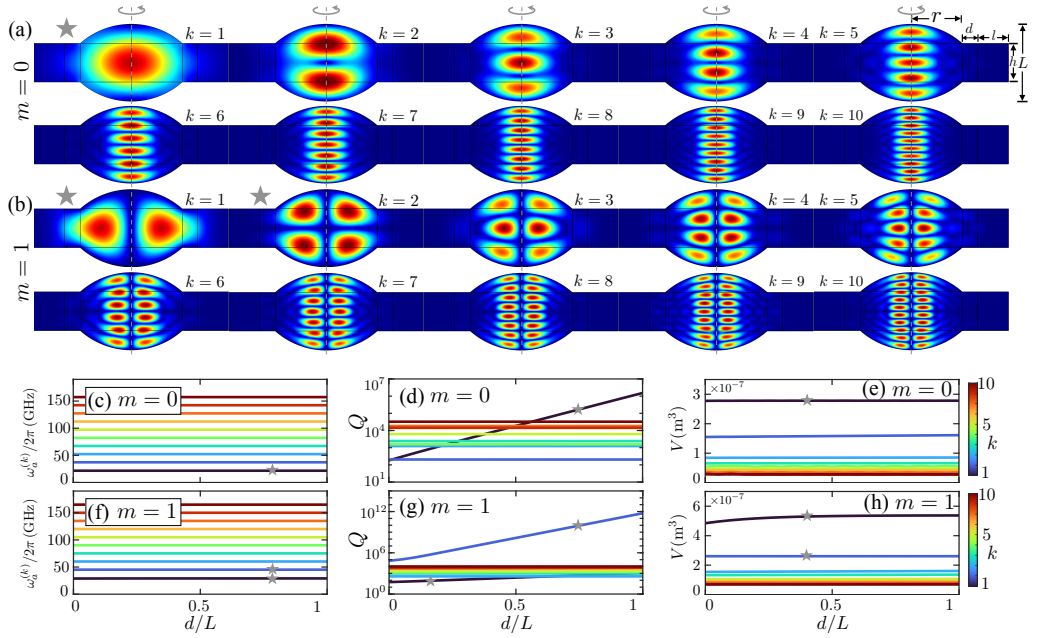

FIG. S2: (a-b) Electric field intensity distributions of the resonant modes with different transverse mode orders m and longitudinal mode orders k of the specially designed Fabry–Pérot cavity when the wing width $d = 0.2L$, where l is the width of perfectly matched layers. (c-h) Resonant frequencies $\omega_a^{(k)}/2\pi$, quality factor Q, and mode volume V of the cavity versus d/L for different m and k. The geometric parameters of the cavity used here are: $L = 1\,\mathrm{cm}$, $h = 0.5L$, $l = 0.4L$, $r = \sqrt{L^2 - (L/2 + h/2)^2}$, and the curved mirror curvature radiuses $R_1 = R_2 = L$.

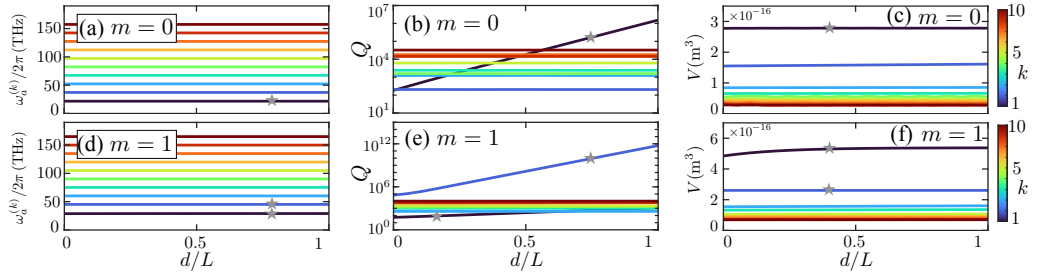

FIG. S3: (a,d) Resonant frequencies $\omega_a^{(k)}/2\pi$, (b,e) quality factor Q, and (c,f) mode volume V of the cavity versus d/L for different m and k. The geometric parameters of the cavity used here are: $L = 10\,\mathrm{um}$, $h = 0.5L$, $l = 0.4L$, $r = \sqrt{L^2 - (L/2 + h/2)^2}$, and the curved mirror curvature radiuses $R_1 = R_2 = L$.

the resonant frequencies, quality factor, and mode volume of such micrometer size cavities. Similar to their centimeter-scale counterparts, the resonant frequency in the micrometer-scale cavities can also be expressed as $\omega_a^{(k)}/2\pi = c[k + (m+1)/2]/(2\eta L)$, and are nearly unaffected by variations in the wing width d. The trends of the resonant frequencies $\omega_a^{(k)}$ and mode volume V with respect to d closely follow those observed in the centimeter-scale case. However, the absolute values differ: the resonant frequencies $\omega_a^{(k)}$ are approximately three orders of magnitude higher, and the mode volumes V are about nine orders of magnitude smaller compared to the centimeter-scale cavities. Despite this size reduction, the quality factor Q remains nearly the same. These results confirm that the proposed method—enhancing cooperativity by adding wings and tuning the wing width—is equally effective at different cavity scales, including micrometer-scale cavities.

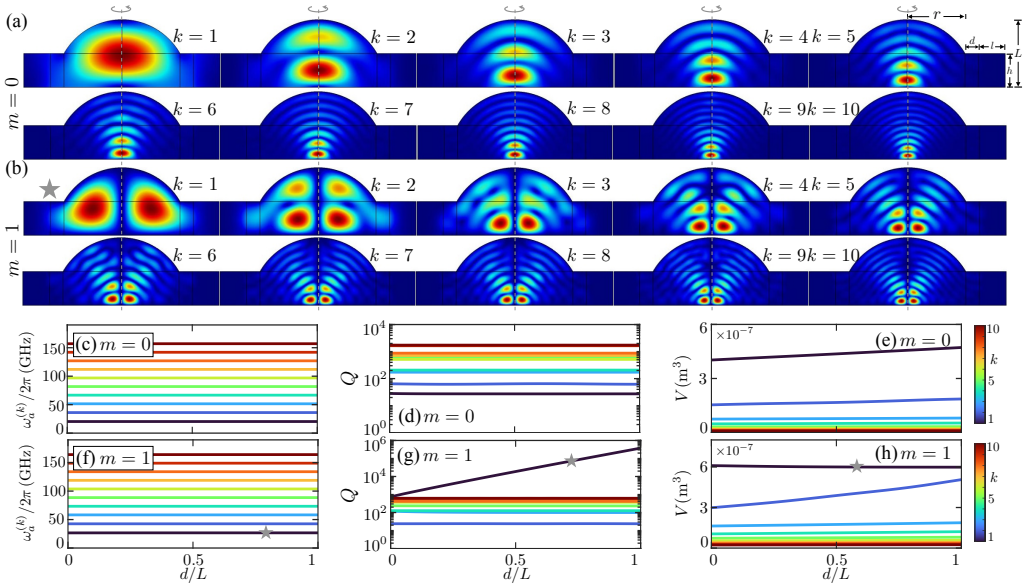

FIG. S4: (a-b) Electric field intensity distributions of the resonant modes with different transverse mode orders m and longitudinal mode orders k of the specially designed cavity when the wing width $d = 0.2L$, where l is the width of perfectly matched layers. (c)-(h) Resonant frequencies $\omega_a^{(k)}/2\pi$, quality factor Q, and mode volume V of the cavity versus d/L for different m and k. The geometric parameters of the cavity used here are: $L = 1\,\mathrm{cm}$, $h = 0.5L$, $l = 0.4L$, $r = \sqrt{L^2 - h^2}$, and the curved mirror curvature radiuses $R_1 = L$ and $R_2 = \infty$.

III. WINGED MICRODOME FABRY–PÉROT CAVITIES

Figure S4 displays the properties of a winged microdome Fabry–Pérot cavity. This Fabry–Pérot cavity consists of two mirrors with additional wing width d, and the maximum and minimum distances between the mirrors are L and h, respectively. When the wing width $d/L = 0$, the microdome cavity corresponds to a standard semi-concentric Fabry–Pérot cavity, where the radius of curvature R_1 of one mirror is equal to the cavity length L, while the radius of curvature of the other mirror $R_2 = \infty$. Figures S4(a) and S4(b) show the electric field intensity distributions of the resonant modes with small longitudinal mode orders k when the transverse mode orders are $m = 0$ and $m = 1$, respectively. These electric field intensity distributions are primarily confined to the microdome region of the cavity rather than extending into the wings. The corresponding resonant frequencies of the winged semi-concentric Fabry–Pérot cavity are the same as those of the symmetric confocal Fabry–Pérot cavity, given by $\omega_a^{(k)}/2\pi = c[k + (m+1)/2]/(2\eta L)$, as shown in Figs. S4(c) and S4(f). These resonant frequencies depend on the mode order m and k, as well as cavity geometry through L, but are not influenced by the wing width d.

The mode volume V for different modes are displayed in Figs. S4(e) and S4(h), where V remains unchanged with increasing d. This is because the geometry of this cavity enhances the electric field intensities without significantly altering the electric field distributions. Specially, in the winged microdome cavity, there still exists a mode with $m = 1, k = 1$ (corresponding to the subwavelength light modes), whose quality factor Q improves almost exponentially with the wing width d, as indicated by the asterisks in Fig. S4(g). However, the Q value for the $m = 1, k = 1$ mode in the winged microdome cavity is lower than that of the $m = 0, k = 1$ and $m = 1, k = 2$ modes in the winged symmetric confocal Fabry–Pérot cavities. This is attributed to the weaker confinement of the electric field within the dome region and its greater extension into the wings in the microdome cavity, as shown in Figs. S2(a,b) and S4(b), which leads to increased geometric losses. Overall, the winged microdome cavity can also overcome the typical trade-off between achieving a high quality factor Q and maintaining a small mode volume V. Therefore, we predict that the Q/V ratio and the single-atom cooperativity parameter $\mathcal{C}$ can also be improved almost exponentially with increasing wing width d in this cavity QED system.

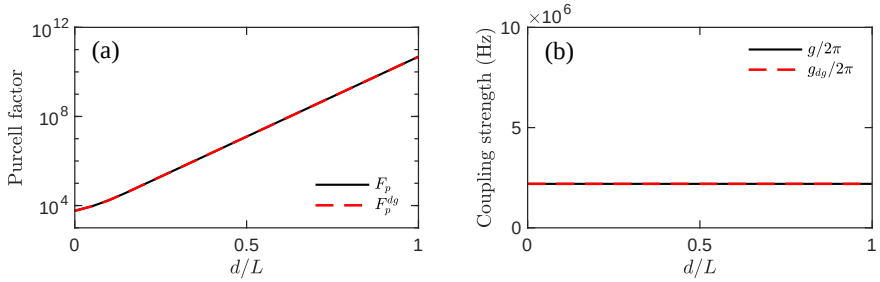

FIG. S5: (a,b) Purcell factor and coupling rate versus d/L in the ideal winged symmetric confocal Fabry–Pérot cavity. The black solid lines and red dashed lines represent the results obtained using the simplified single high-Q mode approximation and the Green's dyadic approach, respectively. The selected cavity mode corresponds to $m = 1$ and $k = 2$. System parameters used here are: $\omega_a/2\pi = \omega_\sigma/2\pi = 45.2\,\mathrm{GHz}$ and $\gamma/2\pi = 2.5 \times 10^3$ Hz.

IV. LOCAL COUPLING AND PURCELL ENHANCEMENT

In the main text, the coupling rate g between a single atom and a cavity mode is given by [1, 2]

$$g = \gamma\sqrt{\frac{\mathbb{V}_a}{V}} = \sqrt{\frac{3\pi c^3\gamma}{\omega_\sigma^2 V}} \tag{S1}$$

assuming the atom is placed at the location of maximum electric field strength. Here, $\mathbb{V}_a = 3\pi c^3/(\gamma\omega_\sigma^2)$ is the characteristic atomic interaction volume. The mode volume is approximately defined as $V = \int_{\mathcal{V}} \epsilon(\mathbf{r})|\mathbf{E}(\mathbf{r})|^2/\max[\epsilon(\mathbf{r})|\mathbf{E}(\mathbf{r})|^2]d^3\mathbf{r}$. These simplified expressions for the mode volume and coupling rate serve as reasonable approximations for high-Q cavity modes. To verify the validity of this approximation in our model, we next present a rigorous estimate of the local coupling rate and Purcell enhancement via the Green's dyadic.

The Purcell factor is defined as $F_p = \Gamma_{\mathrm{cav}}/\Gamma_0$, where the free-space spontaneous emission rate is

$$\Gamma_0 = \frac{\omega_\sigma^3}{3\pi\hbar\epsilon_0 c^3}|\mathbf{d}|^2, \tag{S2}$$

where ω_σ is the transition frequency of the atom, $\mathbf{d}$ is the dipole moment of the atom. The spontaneous emission rate of the atom in the cavity Γ_{cav} is given by

$$\Gamma_{\mathrm{cav}} = \frac{\pi\omega_\sigma}{\hbar\epsilon_0}|\mathbf{d}|^2\rho_d(\mathbf{r}_0,\omega_\sigma), \tag{S3}$$

where $\rho_d(\mathbf{r}_0,\omega_\sigma)$ is the projection local density of states, related to the dyadic Green's function

$$\rho_d(\mathbf{r}_0,\omega_\sigma) = \frac{2\omega_\sigma}{\pi c^2}\mathrm{Im}\left[\mathbf{e}\cdot\mathbf{G}(\mathbf{r}_0,\mathbf{r}_0;\omega_\sigma)\cdot\mathbf{e}\right], \tag{S4}$$

where $\mathbf{e}$ is a unit vector in the direction of the dipole moment. The dyadic Green's function can be expressed in terms of the cavity eigenmodes as [3, 4]

$$\mathbf{G}(\mathbf{r}_0,\mathbf{r}_0;\omega_\sigma) = c^2\sum_n \frac{\mathbf{E}_n(\mathbf{r}_0)\bigotimes\mathbf{E}_n^*(\mathbf{r}_0)}{2\tilde{\omega}_{a,n}(\tilde{\omega}_{a,n}-\omega_\sigma)}, \tag{S5}$$

where $\tilde{\omega}_{a,n}$ is the complex resonance frequency of the n-th mode, $\omega_{a,n}$ is its real part, $\kappa_n = \omega_{a,n}/(2Q)$ is its imaginary part, and $\mathbf{E}_n(\mathbf{r})$ is the normalized electric field of the nth mode, such that $\int\epsilon(\mathbf{r})|\mathbf{E}_n(\mathbf{r})|^2dV = \int|\mathbf{E}_n(\mathbf{r})|^2dV = 1$. Thus we have

$$\begin{aligned}\mathbf{e}\cdot\mathbf{G}(\mathbf{r}_0,\mathbf{r}_0;\omega_\sigma)\cdot\mathbf{e} &= \mathbf{e}\cdot\sum_n\frac{c^2\mathbf{E}_n(\mathbf{r}_0)\bigotimes\mathbf{E}_n^*(\mathbf{r}_0)}{2\tilde{\omega}_{a,n}(\tilde{\omega}_{a,n}-\omega_\sigma)}\cdot\mathbf{e} = \frac{c^2}{2}\sum_n|\mathbf{e}\cdot\mathbf{E}_n(\mathbf{r}_0)|^2\frac{1}{\tilde{\omega}_{a,n}(\tilde{\omega}_{a,n}-\omega_\sigma)}\\ &= -\frac{c^2}{2}\sum_n|\mathbf{e}\cdot\mathbf{E}_n(\mathbf{r}_0)|^2\frac{i\kappa_n(\omega_\sigma-\omega_{a,n})-i\kappa_n\omega_{a,n}+\omega_{a,n}(\omega_\sigma-\omega_{a,n})+\kappa_n^2}{(\omega_{a,n}^2+\kappa_n^2)[(\omega_\sigma-\omega_{a,n})^2+\kappa_n^2]}.\end{aligned} \tag{S6}$$

Inserting this equation into the Purcell factor formula gives

$$F_p^{dg} = \frac{\Gamma_{\text{cav}}}{\Gamma_0} = \frac{6\pi c}{\omega_\sigma}\text{Im}\left[\mathbf{e}\cdot\mathbf{G}(\mathbf{r}_0,\mathbf{r}_0;\omega_\sigma)\cdot\mathbf{e}\right] = \frac{6\pi c}{\omega_\sigma}\frac{c^2}{2}\sum_n |\mathbf{e}\cdot\mathbf{E}_n(\mathbf{r}_0)|^2 \frac{\kappa_n(2\omega_{a,n}-\omega_\sigma)}{(\omega_{a,n}^2+\kappa_n^2)[(\omega_\sigma-\omega_{a,n})^2+\kappa_n^2]}$$
$$= \frac{3\pi c^3}{\omega_\sigma}\sum_n |\mathbf{e}\cdot\mathbf{E}_n(\mathbf{r}_0)|^2 \frac{\kappa_n(2\omega_{a,n}-\omega_\sigma)}{(\omega_{a,n}^2+\kappa_n^2)[(\omega_\sigma-\omega_{a,n})^2+\kappa_n^2]}. \tag{S7}$$

For a single high-Q cavity mode on resonance with the atomic transition ($\omega_\sigma = \omega_{a,n} \gg \kappa_n$), and approximating $\omega_{a,n}^2+\kappa_n^2 \approx \omega_{a,n}^2$, the Purcell factor simplifies to

$$F_p^{dg} \approx \frac{3\pi c^3}{\omega_\sigma}\frac{|\mathbf{e}\cdot\mathbf{E}_n(\mathbf{r}_0)|^2}{\omega_\sigma\kappa_n}. \tag{S8}$$

Assuming the atom is located at the location of maximum electric field strength, we have

$$|\mathbf{e}\cdot\mathbf{E}_n(\mathbf{r}_0)|^2 = \max[|\mathbf{E}_n(\mathbf{r})|^2] = \frac{1}{V_n}, \tag{S9}$$

where the effective mode volume $V_n = \int_{\mathcal{V}} \epsilon(\mathbf{r})|\mathbf{E}_n(\mathbf{r})|^2/\max[\epsilon(\mathbf{r})|\mathbf{E}_n(\mathbf{r})|^2]d^3\mathbf{r} = 1/\max[|\mathbf{E}_n(\mathbf{r})|^2]$. Substituting Eq. (S9) into Eq. (S8), the Purcell factor expression for a single high-Q mode can be simplified as

$$F_p^{dg} \approx \frac{3\pi c^3}{\omega_\sigma^2\kappa_n V_n} = \frac{6\pi c^3 Q}{\omega_\sigma^3 V_n} = \frac{3Q\lambda^3}{4\pi^2 V_n} = \frac{3\lambda^3}{4\pi^2}\frac{Q}{V_n} = F_p', \tag{S10}$$

which coincides with the classic Purcell factor expression $F_p' = 3\lambda^3 Q/(4\pi^2 V_n)$. Figure S5(a) compares the Purcell factor calculated from the simplified single-mode expression F_p' in Eq. (S10) (black solid line) with that obtained from the rigorous Green's dyadic approach in Eq. (S7) (red dashed line). The close agreement between the two methods confirms the validity of the simplified approximation based on a single high-Q mode in our system.

We now focus on the local coupling strength between an atom that is resonantly coupled to a single cavity mode with resonance frequency $\omega_{a,n}$ (i.e., $\omega_\sigma = \omega_{a,n}$). Based on the above discussions, the coupling strength is given by

$$g_{dg} = \sqrt{\frac{|d|^2\omega_\sigma^3}{\hbar\epsilon_0(\omega_\sigma^2+\kappa_n^2)}|\mathbf{e}\cdot\mathbf{E}_n(\mathbf{r}_0)|^2} = \sqrt{\frac{3\pi c^3\gamma}{\omega_\sigma^2+\kappa_n^2}|\mathbf{e}\cdot\mathbf{E}_n(\mathbf{r}_0)|^2}. \tag{S11}$$

where we used $|d|^2 = 3\pi\epsilon_0\hbar c^3\gamma/\omega_\sigma^3$ for the electric dipole of the atom. For a high-Q cavity mode with $\omega_\sigma = \omega_{a,n} \gg \kappa_n$, the denominator simplifies as $\omega_\sigma^2+\kappa_n^2 \approx \omega_\sigma^2$, leading to

$$g_{dg} \approx \sqrt{\frac{3\pi c^3\gamma}{\omega_\sigma^2 V_n}} = \gamma\sqrt{\frac{\mathbb{V}_a}{V_n}} = g, \tag{S12}$$

which is consistent with Eq. (S1). Figure S5(b) shows the coupling strength calculated using the simplified expression g from Eq. (S1) (black solid line), along with the rigorous Green's dyadic result from Eq. (S11) (red dashed line). The close match between the two again confirms the validity of the simplified single high-Q mode approximation employed in our system.

[S1] S.M. Spillane, T.J. Kippenberg, K.J. Vahala, K.W. Goh, E. Wilcut, and H.J. Kimble, Ultrahigh-Q toroidal microresonators for cavity quantum electrodynamics, Phys. Rev. A **71**, 013817 (2005).

[S2] K. Srinivasan, M. Borselli, O. Painter, A. Stintz, and S. Krishna, Cavity Q, mode volume, and lasing threshold in small diameter AlGaAs microdisks with embedded quantum dots, Opt. Express **14**, 1049 (2006).

[S3] P.T. Kristensen and S. Hughes, Modes and Mode Volumes of Leaky Optical Cavities and Plasmonic NanoresonatorsArticle link copied, ACS Photonics **1**, 2(2014).

[S4] P. Lalanne, W. Yan, K. Vynck, C. Sauvan, J.-P. Hugonin, Light Interaction with Photonic and Plasmonic Resonances, Laser Photonics Rev. **12**, 1700113 (2018).